Electronic structures and optical properties of Zn-doped β-Ga_2O_3 with different doping sites*

Li Chao(李 超), Yan Jin-Liang (闫金良)†, Zhang Li-Ying(张丽英), and Zhao Gang(赵 刚)

School of Physics and Optoelectronic Engineering, Ludong University, Yantai 264025, *China*

(Received 6 April 2012; revised manuscript received 22 May 2012)

The electronic structures and optical properties of intrinsic β-Ga_2O_3 and Zn-doped β-Ga_2O_3 are investigated by first-principles calculations. The analysis about the thermal stability shows that Zn-doped β-Ga_2O_3 remains stable. The Zn doping does not change the basic electronic structure of β-Ga_2O_3, but only generates an empty energy level above the maximum of the valence band, which is shallow enough to make the Zn-doped β-Ga_2O_3 a typical p-type semiconductor. Because of Zn doping, absorption and reflectivity are enhanced in the near infrared region. The higher absorption and reflectivity of $Zn_{Ga(2)}$ than those of $Zn_{Ga(1)}$ are due to more empty energy states of $Zn_{Ga(2)}$ than those of $Zn_{Ga(1)}$ near E_f in the near infrared region.

Keywords: first-principles, Zn-doped β-Ga_2O_3, p-type semiconductor, optical properties

PACS: 71.20.–b, 71.15.Dx, 71.55.–I, 71.55.Eq **DOI:** 10.1088/1674-1056/21/12/127104

1. Introduction

Monoclinic gallium oxide (β-Ga_2O_3) is an insulator with a band gap of 4.9 eV,[1] and it exhibits n-type semiconducting properties at high temperature.[2] In recent years, thin films and single crystals of β-Ga_2O_3 have received significant attention. β-Ga_2O_3 nanobelts were synthesized by thermal evaporation and their NO_2 sensing properties were studied at room temperature.[3] β-Ga_2O_3 thin films were deposited on 6H–SiC substrates through the radio frequency magnetron sputtering for the application of SiC-based devices with Ga_2O_3.[4] The β-Ga_2O_3 thin films have numerous applications in semiconducting laser,[5] high temperature oxygen sensor,[6] and UV-transparent conductive oxide,[7] and so on. To improve its electrical properties and versatility in making electronic devices, p-type doping is very important. Liu *et al.*[8] fabricated p-type N-doped β-Ga_2O_3 nanowires with the CVD method via reacting Ga_2O_3 powders with NH_3. Zhang *et al.*[9,10] investigated N-doped β-Ga_2O_3 and N–Zn co-doped β-Ga_2O_3 by first principles calculation, and they found that one acceptor impurity level is at about 0.761 eV above the valence band in N-doped β-Ga_2O_3 and two impurity levels are at about 0.149 eV and 0.483 eV above the valence band in N–Zn co-doped β-Ga_2O_3. Because of the similar ionic sizes of Zn and Ga atoms (Zn^{2+}: 0.074 nm, Ga^{3+}: 0.062 nm), the Zn atom is a good candidate of substitution for doping of the Ga atom. Recently, Chang *et al.*[11] synthesized quasi-one-dimensional Zn-doped β-Ga_2O_3 nanowires via catalytic chemical vapour deposition method, which showed that Zn-doped β-Ga_2O_3 nanowires exhibit p-type semiconducting behaviour with the enhancement of conductivity. However, to date few theoretical investigations on Zn-doped β-Ga_2O_3 have been reported to reveal the origin of its outstanding properties caused by the doping of Zn. In this paper, we focus on the doping effect of Zn substituting different Ga sites on the structural, electronic, and optical properties of Zn-doped β-Ga_2O_3 to obtain some explanations and even guidelines for future experimental work.

2. Method and model

First principles calculations based on the density functional theory (DFT) have been performed using the CASTEP code.[12] The electron–electron exchange and correlation effects are described by Perdew–Burke–Ernzerhof (PBE) in generalized gra-

*Project supported by the National Natural Science Foundation of China (Grant No. 10974077), the Natural Science Foundation of Shandong Province, China (Grant No. 2009ZRB01702), and the Shandong Provincial Higher Educational Science and Technology Program, China (Grant No. J10LA08).

†Corresponding author. E-mail: yanjinliang@yahoo.cn

© 2012 Chinese Physical Society and IOP Publishing Ltd

dient approximation (GGA).[13] Ultrasoft pseudopotentials,[14] known for their high efficiency in calculating the structural and electronic properties, are utilized for the electron–ion interactions. In our calculation, a 2×4×2 k-point Monkhorst Pack mesh[15] in the Brillouin zone is used, and the self-consistent calculations are carried out using a convergence criterion of 5.0×10^{-7} eV/atom and a cutoff energy of 380 eV. All atoms are allowed to relax until the force on each atom is below 0.01 eV/Å (1 Å=0.1 nm) and the displacement of each atom is below 5.0×10^{-4} Å. The electronic states of $2s^22p^4$, $3d^{10}4s^24p^1$, and $3d^{10}4s^2$ are considered as the valence states for O, Ga, and Zn, respectively.

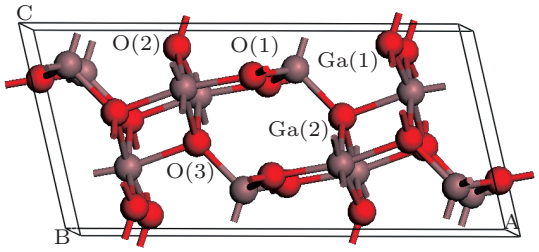


Fig. 1. (colour online) Crystal structure of β-Ga_2O_3.

The crystal structure of β-Ga_2O_3 is shown in Fig. 1. There are two different Ga sites, denoted as Ga(1) and Ga(2), and three different O sites, denoted as O(1), O(2), and O(3).[16] The β-Ga_2O_3 belongs to space group $C2/m$ with two-fold rotation axis b.[17] Ga atoms are surrounded by O atoms in either tetrahedral Ga(1) or octahedral Ga(2) coordination. In this work, a 1×2×2 supercell containing 80 atoms is used to model the Zn-doped β-Ga_2O_3, in which a Ga atom is substituted by one Zn atom. This corresponds to a doping concentration of 2 wt%. The Ga atoms have two different sites, so there are two configurations of $ZnGa_{31}O_{48}$, namely, $Zn_{Ga(1)}$ and $Zn_{Ga(2)}$.

3. Results and discussion

3.1. Structural properties

At first, the geometry optimization is performed using the BFGS minimization algorithm.[18] The equilibrium structures are obtained after the cell geometry and volume have been fully relaxed by minimizing the total energy and forces. The relaxed lattice constants of intrinsic β-Ga_2O_3 and Zn-doped β-Ga_2O_3 are shown in Table 1. The calculated results of intrinsic β-Ga_2O_3 are consistent with the theoretical values in Ref. [19]. For $Zn_{Ga(1)}$, because the ionic radius of Zn^{2+} is larger than that of Ga^{3+}, the lattice parameters a, b, c, and the cell volume V increase. The same reason can explain why the lattice parameters a and b in the configuration $Zn_{Ga(2)}$ increase. However the lattice parameter c of $Zn_{Ga(2)}$ decreases slightly, which is mainly attributed to the variation of the bond angle O(2)–Ga(2)–O(3) in y–z plane from 80.92° to 79.91°.

Table 1. Structural parameters and values of standard enthalpy of formation (ΔH_f) for intrinsic β-Ga_2O_3 and Zn-doped β-Ga_2O_3.

	a/Å	b/Å	c/Å	α	β	γ	V/Å^3	ΔH/eV
Intrinsic β-Ga_2O_3	12.498	6.191	11.796	90.000	103.696	90.000	886.834	–11.02
$Zn_{Ga(1)}$	12.591	6.203	11.804	90.000	103.608	90.000	896.119	–10.83
$Zn_{Ga(2)}$	12.533	6.194	11.793	90.000	103.615	90.000	889. 741	–10.83

The structural distortion caused by Zn doping deteriorates the stability of Zn-doped β-Ga_2O_3, which is revealed by the standard enthalpy of formation (ΔH_f).[20] The ΔH_f denotes the enthalpy change associated with the formation of a compound from its constituent elements with all substances in their standard states. Using a method similar to that in Ref. [21], the ΔH_f is determined as

$$\Delta H_f\,(Zn_xGa_{2-x}O_3) = x\mu_{Zn} + (2-x)\,\mu_{Ga} + 3\mu_O, \quad (1)$$

where the chemical potentials $\mu_{Ga[bulk]}$, $\mu_{O[O2]}$, and $\mu_{Zn[bulk]}$ refer to the calculated total energies of Ga in β-Ga [$E_{tot}(Ga^0)$], O in O_2 molecules [$1/2E_{tot}(O_2)$], and Zn in bulk Zn [$E_{tot}(Zn^0)$], respectively. The values of ΔH_f for the configurations $Zn_{Ga(1)}$ and $Zn_{Ga(2)}$ are listed in Table 1. The calculated value of ΔH_f for intrinsic β-Ga_2O_3 is −11.02 eV, close to the experiment value of −11.29 eV,[22] and the error in our calculation is 2.39%. The values of ΔH_f of configurations $Zn_{Ga(1)}$ and $Zn_{Ga(2)}$ have the same value of −10.83 eV. With the introduction of Zn, ΔH_f is reduced slightly. The same ΔH_f shows that two configurations $Zn_{Ga(1)}$ and $Zn_{Ga(2)}$ have the same thermal stabilities. Furthermore, because bigger ΔH_f means

more stable crystal structure,[23] the structural stabilities of the configurations $Zn_{Ga(1)}$ and $Zn_{Ga(2)}$ are reduced in comparison with that of intrinsic β-Ga_2O_3, but they are still stable.

3.2. Charge density

Figure 2 is the contour plots of the electron density difference between intrinsic β-Ga_2O_3 and Zn-doped β-Ga_2O_3 on (010) plane. The density difference distributions can be used to analyse bonding characteristics in the crystal. The ionic or covalent character in β-Ga_2O_3 has important information to explain the transport property in these materials and is a somewhat controversial topic.[24] In Fig. 2(a), there is an accumulation of electronic density in the region between the Ga(1) atom and its nearest oxygen atoms. Some electron density is removed from the region around the nuclei of the O atom and is added to the region between the O atom and the nearest Ga(1) atom. So the higher degree of covalence is associated with Ga(1)–O bonds. However, due to its higher coordination of Ga(2) in the crystalline lattice, it is observed from Fig. 2(b) that electron density is removed from the region around the Ga(2) atom and is added to the spherical region around its nearest neighbour O atom. It displays ionic bonding characteristics between the Ga(2) and its nearest neighbour O atoms. The density difference of Ga(1) and Ga(2) atoms in intrinsic β-Ga_2O_3 presents a spherical distribution, which means only the outer shell electrons ($4s^24p^1$) of Ga atoms are lost and bonded with neighbouring O atoms.

With the introduction of Zn impurity, some changes in the charge density distribution are observed in Figs. 2(c) and 2(d). Due to the fact that the electronegativity of the Zn atom is lower than that of the Ga atom and the valence electrons of the Zn atom are less than those of the Ga atom, the Zn atom loses almost all valence electrons while the electron density around the O atoms increases obviously. The electron density in the region between the Zn atom and the nearest O atom is reduced further. It demonstrates that there is strong ionic bonding between Zn and nearest neighbour O atoms.

The density difference of Zn atoms in Zn-doped β-Ga_2O_3 shows apparent polar distributions, which means all the outer shell electrons ($4s^2$) and partial inner $3d^{10}$ electrons of Zn atoms are coupled with O 2p electrons in Zn-doped β-Ga_2O_3.

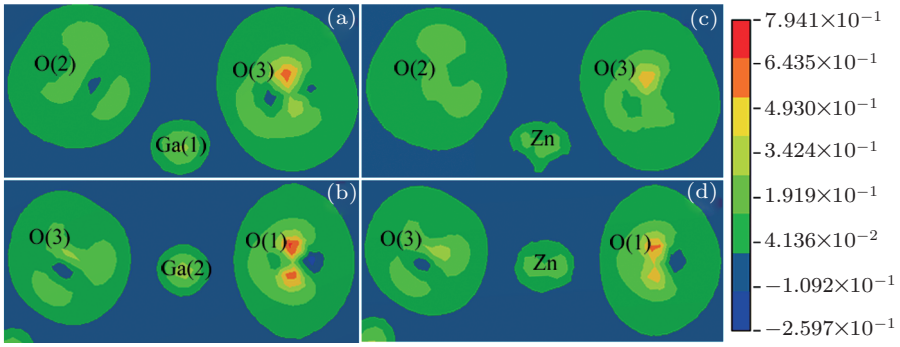


Fig. 2. (colour online) Electron density difference between intrinsic β-Ga_2O_3 and Zn-doped β-Ga_2O_3 on (010) plane. (a) Ga(1), (b) Ga(2), (c) $Zn_{Ga(1)}$, and (d) $Zn_{Ga(2)}$. Positive values indicate the accumulation of electronic charge; negative values correspond to depletion of charge.

3.3. Band structure and density of states

Figure 3 shows the energy band structure of intrinsic β-Ga_2O_3 at high symmetry point across the first Brillouin zone. The E_f is set at the zero-point of the energy scale. The calculated band gap is smaller than the experimental band gap. It is because DFT theory is based on the ground state theory, in which the exchange–correlation potential of the excited electrons is underestimated. However, in the same computing conditions, it would not affect the analysis of electronic structure. Band structure shows that the valance bands are divided into three regions: the upper valence band from −6.77 eV to 0.0 eV, middle valence band from −12.88 eV to −11.63 eV, and the lower one from −16.83 eV to −18.53 eV. It is known that the material properties are determined mainly by the upper valence band and the conduction band. So we will not discuss the middle valence band and the lower valence band here. Total density of states

(TDOS) and partial density of states (PDOS) of intrinsic β-Ga_2O_3 as seen in Fig. 4, indicate that the upper valence band is composed of Ga 4s, Ga 4p, and O 2p states. Furthermore, the top of the valence band is formed by the O 2p states, while the bottom of the conduction band is composed of the Ga 4s states. The results are consistent with other calculations.[19,25]

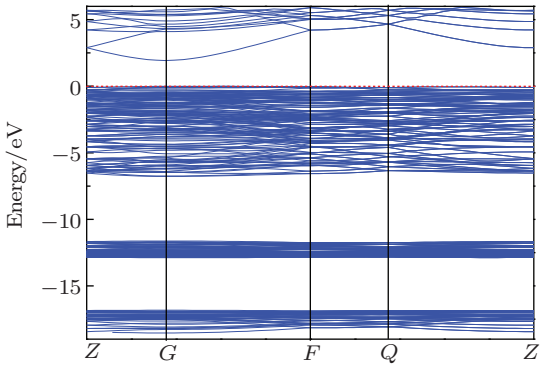


Fig. 3. (colour online) Band structure of intrinsic β-Ga_2O_3. The top of the valence band is aligned to zero level.

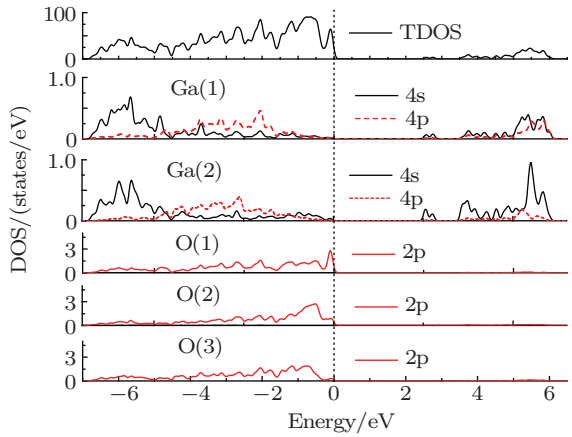


Fig. 4. (colour online) TDOSs and PDOSs of intrinsic β-Ga_2O_3. The Fermi level is set at the zero-point of the energy scale.

Figures 5(a) and 5 (b) show the calculated band structures near the top of the valence band of two configurations $Zn_{Ga(1)}$ and $Zn_{Ga(2)}$, respectively. The acceptor level is at 0.07 eV above the top of the valence band for $Zn_{Ga(1)}$ while it is at 0.05 eV above the top of the valence band for $Zn_{Ga(2)}$. Acceptor levels of N-doped β-Ga_2O_3 at about 0.761 eV above the valence band[9] at the Z-point and acceptor levels of N–Zn co-doped β-Ga_2O_3 at about 0.149 eV above the valence band[10] at the Q-point were reported, which are too deep to be thermally excited at room temperature. The acceptor levels of Zn-doped β-Ga_2O_3 are shallow enough for electrons to be thermally excited from the valence band to acceptor levels to make it a β typical p-type semiconductor. However, figure 5 shows the tops of the valence band for two configurations $Zn_{Ga(1)}$ and $Zn_{Ga(2)}$ are almost flat, indicating a rather large effective mass (m_h^*) of holes.[26] Consequently, in terms of the inverse relation between hole mobility and effective mass m_h^*, the large m_h^* is one of the reasons for the low mobility of Zn-doped β-Ga_2O_3 in experiment.[11]

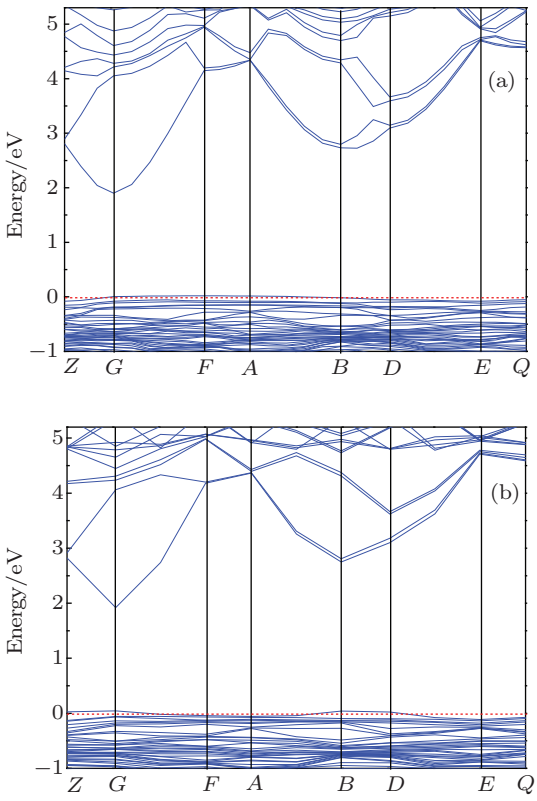


Fig. 5. (colour online) Band structures near the top of the valence band of configurations $Zn_{Ga(1)}$ (a) and $Zn_{Ga(2)}$ (b), in which the short dashed lines represent the Fermi level set to zero.

The details of the TDOSs and PDOSs of two configurations $Zn_{Ga(1)}$ and $Zn_{Ga(2)}$ can be found from Figs. 6 and 7, respectively. The introduction of Zn impurity does not change the basic electronic structure of β-Ga_2O_3, but generates the empty energy states above the top of the valence band. The top of the valence band is attributed to the overlap of Zn 3d and O 2p states while the bottom of the conduction band is still formed by Ga 4s states. Furthermore, the empty energy levels are composed of not only Zn 3d but also some O 2p states in both configurations $Zn_{Ga(1)}$ and $Zn_{Ga(2)}$. However, there are more empty Zn 3d states near E_f in the configuration $Zn_{Ga(2)}$ than in the $Zn_{Ga(1)}$. Because of the lower electro-negativity

of Zn, more electron densities around Zn are transferred to the nearest neighbour O atoms. Therefore, the PDOSs of O 2p states near the top of the valence band of the configurations $Zn_{Ga(1)}$ and $Zn_{Ga(2)}$ are enhanced obviously compared with that of intrinsic β-Ga_2O_3.

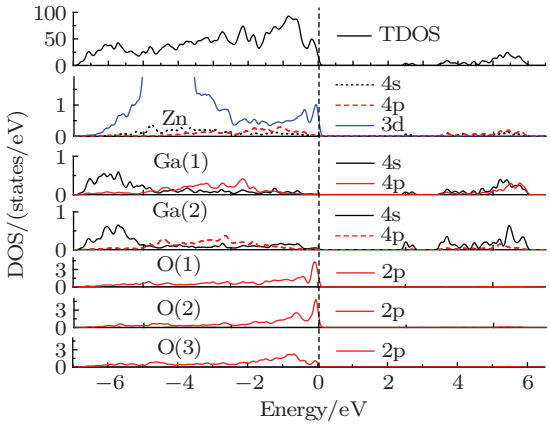


Fig. 6. (colour online) TDOSs and PDOSs of the configuration $Zn_{Ga(1)}$. The E_f is set at the zero-point of the energy scale.

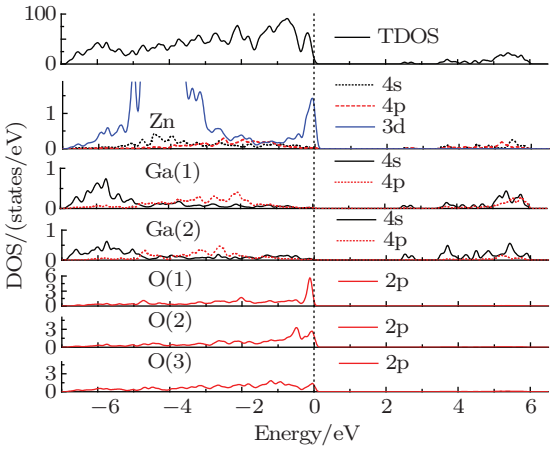


Fig. 7. (colour online) TDOSs and PDOSs of the configuration $Zn_{Ga(2)}$. The E_f is set at the zero-point of the energy scale.

3.4. Optical properties

It is known that the optical properties, such as absorption and reflectivity, can be derived from the dielectric function $\varepsilon(\omega) = \varepsilon_1(\omega) + i\varepsilon_2(\omega)$, where $\varepsilon_2(\omega)$ is thought of as the real transition between occupied electronic states and unoccupied electronic states and can be obtained directly from the CASTEP code;[27] $\varepsilon_1(\omega)$ can be evaluated from imaginary part $\varepsilon_2(\omega)$ through the Kramer–Kronig relationship. A total of 100 empty bands are included in the optical calculation which is performed using the polycrystalline polarization where the E field vector is an isotropic average over all directions. No significant difference in the convergence is found by choosing the cutoff energy 400 eV. In addition, the band gap is underestimated by GGA based on DFT, which causes a notable red-shift of optical spectra.

The calculated optical absorptions and reflectivity spectra of intrinsic β-Ga_2O_3 and two configurations $Zn_{Ga(1)}$ and $Zn_{Ga(2)}$ are shown in Fig. 8 and Fig. 9, respectively. The band gap and the main shapes of the valence and conduction bands change slightly with increasing Zn doping. Since the optical absorption of the semiconductor originates mainly from the interband electron excitation between the valence band and the conduction band, the stabilities of the valence band and conduction band will result in the unchanged $\varepsilon_2(\omega)$, absorption, and reflectivity spectra in the UV region. According to the selection rules of dipole transitions, $\Delta L = \pm 1$,[28] the absorption in the UV region corresponds mainly to interband transition from O 2p states in the upper valence band to the empty Ga 4s states in the conduction band for intrinsic and Zn-doped β-Ga_2O_3. In addition, the slight fluctuation of absorption for configurations $Zn_{Ga(1)}$ and $Zn_{Ga(2)}$ in the UV region is attributed to the transition from Zn 3d states in the valence band to Ga 4p states in the conduction band. On the other hand, the empty energy levels appearing above E_f caused by Zn doping lead to the transitions from the top of the valence band to these empty levels, resulting in the elevated $\varepsilon_2(\omega)$ and the consequent enhanced absorption and reflectivity in the near infrared region.

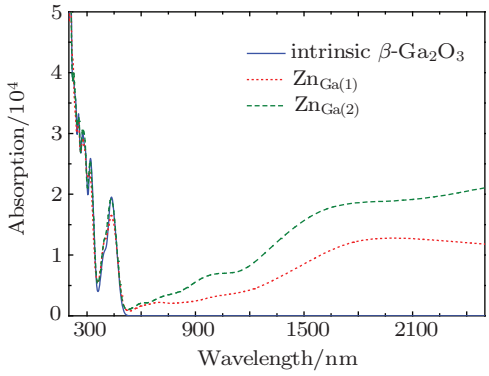


Fig. 8. (colour online) Calculated absorption spectra of intrinsic β-Ga_2O_3 (solid line), configuration $Zn_{Ga(1)}$ (dotted line), and $Zn_{Ga(2)}$ (dashed line).

Furthermore, figure 8 illustrates that the absorption of configuration $Zn_{Ga(2)}$ is stronger than that of $Zn_{Ga(1)}$ in visible and near infrared region. It is attributed mainly to the fact that there are more empty Zn 3d states of $Zn_{Ga(2)}$ near the E_f than those of

$Zn_{Ga(1)}$, which causes more opportunities for transitions from the other part of the valence band to the empty levels in $Zn_{Ga(2)}$. Since there is no free carrier in intrinsic β-Ga_2O_3, the reflectivity of intrinsic β-Ga_2O_3 remains unchanged in the near infrared region. However, for Zn-doped β-Ga_2O_3, the greater number of empty energy states of $Zn_{Ga(2)}$ than of $Zn_{Ga(1)}$ near E_f can form a higher carrier concentration in $Zn_{Ga(2)}$. As a consequence, the reflectivity of $Zn_{Ga(2)}$ is higher than that of $Zn_{Ga(1)}$ in the near infrared region.

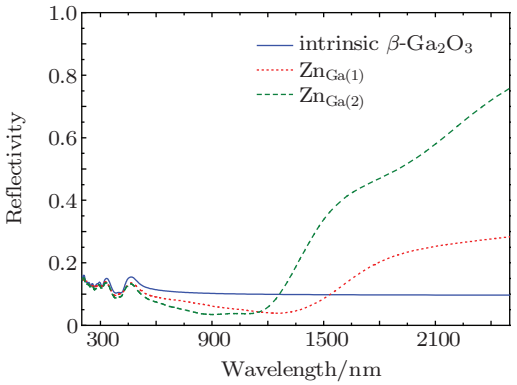


Fig. 9. (colour online) Calculated reflectivity of intrinsic β-Ga_2O_3 (solid line), configuration $Zn_{Ga(1)}$ (dotted line), and $Zn_{Ga(2)}$ (dashed line).

4. Conclusions

The Zn doping does not change the basic electronic structure of β-Ga_2O_3, but generates the acceptor impurity levels at 0.07 eV above the valence band maximum for $Zn_{Ga(1)}$ and at 0.05 eV for $Zn_{Ga(2)}$. The acceptor levels are composed of Zn 3d states and O 2p states in both configurations $Zn_{Ga(1)}$ and $Zn_{Ga(2)}$, but $Zn_{Ga(2)}$ has more empty Zn 3d states near E_f than $Zn_{Ga(1)}$. Correspondingly, absorption and reflectivity in the UV region vary slightly between Zn-doped β-Ga_2O_3 and intrinsic β-Ga_2O_3. Zn-doped β-Ga_2O_3 has strong absorption and reflectivity in the near infrared region, but $Zn_{Ga(2)}$ has higher absorption and reflectivity than $Zn_{Ga(1)}$. Zn-doped β-Ga_2O_3 is a typical p-type semiconductor and has potential applications in UV optoelectronic devices.

References

[1] Wang G T, Xue C S and Yang Z Z 2008 *Chin. Phys.* B **17** 1326
[2] Varley J B, Weber J R, Janotti A and van de Walle C G 2010 *Appl. Phys. Lett.* **97** 142106
[3] Ma H L, Fan D W and Niu X S 2010 *Chin. Phys.* B **19** 076102
[4] Chang S H, Chen Z Z, Huang W, Liu X C, Chen B Y, Li Z Z and Shi E W 2011 *Chin. Phys.* B **20** 116101
[5] Passlacki M, Hong M and Mannaerts J P 1996 *Appl. Phys. Lett.* **68** 1099
[6] Li Y, Trinchi A, Wlodarski W, Galatsis K and Kalantar Z K 2003 *Sens. Actuators* B **93** 431
[7] Medvedeva J E and Chaminda L H 2010 *Phys. Rev.* B **81** 125116
[8] Liu L L, Li M K Yu D Q, Zhang J, Zhang H, Qian C and Yang Z 2010 *Appl. Phys.* A **98** 831
[9] Zhang L Y, Yan J L, Zhang Y J and Li T 2012 *Chin. Phys.* B **21** 067102
[10] Zhang L Y, Yan J L, Zhang Y J, Li T and Ding X W 2012 *Physica* B **407** 1227
[11] Chang P C, Fan Z Y, Tseng W Y, Rajagopal A and Lu J G 2005 *Appl. Phys. Lett.* **87** 222102
[12] Segall M D, Lindan P J D, Probert M J, Pickard C J, Hasnip P J, Clark S J and Payne M C 2002 *J. Phys.: Condens. Matter* **14** 2717
[13] Zhu F, Dong S and Cheng G 2011 *Chin. Phys.* B **20** 077103
[14] Ouyang C Y, Xiong Z H, Ouyang Q Z, Liu G D, Ye Z Q and Lei M S 2006 *Chin. Phys.* **15** 1585
[15] Monkhorst H J and Pack J D 1976 *Phys. Rev.* B **13** 5188
[16] Ahman J, Svensson G and Albertsson J 1996 *Acta Crystallogr.* C **52** 1336
[17] Orita M, Ohta H and Hirano M 2000 *Appl. Phys. Lett.* **77** 25
[18] Fischer T H and Almlof J 1992 *J. Phys. Chem.* **96** 9768
[19] Yoshioka S, Hayashi H, Kuwabara A, Matsunaga K and Tanaka I 2007 *J. Phys.: Condens. Matter* **19** 346211
[20] Feng J, Xiao B, Chen J C and Zhou C J 2009 *Solid State Sci.* **11** 259
[21] Singh A K, Janotti A, Scheffler M and van de Walle C G 2008 *Phys. Rev. Lett.* **101** 055502
[22] Geller S 1960 *J. Chem. Phys.* **33** 676
[23] Feng J, Xiao B, Chen J, Du Y, Yu J and Zhou R 2011 *Materials and Design* **32** 3231
[24] Litimeina F, Racheda D, Khenatab R and Baltacheb H 2009 *J. Alloys Compd.* **9** 20516
[25] He H, Blanco M A and Pandey R 2006 *Appl. Phys. Lett.* **88** 261904
[26] Medvedeva J E, Teasley E N and Hoffman M D 2007 *Phys. Rev.* B **76** 155107
[27] Sheetz R M, Ponomareva I, Richter E, Andriotis A N and Menon M 2009 *Phys. Rev.* B **80** 195314
[28] MacDonald W M 1955 *Phys. Rev.* **98** 60